Nanophase Evolution at Semiconductor/Electrolyte Interface in Situ Probed by Time-Resolved High-Energy Synchrotron X-ray Diffraction

ARTICLE *in* NANO LETTERS · SEPTEMBER 2010

Impact Factor: 13.59 · DOI: 10.1021/nl102458k · Source: PubMed

7 AUTHORS, INCLUDING:

Yugang Sun
Temple University
153 PUBLICATIONS **21,794** CITATIONS
SEE PROFILE

Yang Ren
Argonne National Laboratory
488 PUBLICATIONS **6,231** CITATIONS
SEE PROFILE

Jon D Almer
Argonne National Laboratory
267 PUBLICATIONS **3,054** CITATIONS
SEE PROFILE

Lin Wang
Carnegie Institution for Science
62 PUBLICATIONS **965** CITATIONS
SEE PROFILE

NANO LETTERS

pubs.acs.org/NanoLett

Nanophase Evolution at Semiconductor/Electrolyte Interface in Situ Probed by Time-Resolved High-Energy Synchrotron X-ray Diffraction

Yugang Sun,*,† Yang Ren,‡ Dean R. Haeffner,‡ Jonathan D. Almer,‡ Lin Wang,§ Wenge Yang,§ and Tu T. Truong†

†Center for Nanoscale Materials and ‡X-ray Science Division, Advanced Photon Source, Argonne National Laboratory, 9700 South Cass Avenue, Argonne, Illinois 60439 and §HPSync, Geophysical Laboratory, Carnegie Institute of Washington, 9700 South Cass Avenue, Argonne, Illinois 60439

ABSTRACT Real-time evolution of nanoparticles grown at the semiconductor/electrolyte interface formed between a single crystalline n-type GaAs wafer and an aqueous solution of $AgNO_3$ has been studied by using high-energy synchrotron X-ray diffraction. The results reveal the distinct nucleation and growth steps involved in the growth of anisotropic Ag nanoplates on the surface of the GaAs wafer. For the first time, a quick transit stage is observed to be responsible for the structural transformation of the nuclei to form structurally stable seeds that are critical for guiding their anisotropic growth into nanoplates. Reaction between a GaAs wafer and $AgNO_3$ solution at room temperature primarily produces Ag nanoplates on the surface of the GaAs wafer in the dark and at room temperature. In contrast, X-ray irradiation can induce charge separation in the GaAs wafer to drive the growth of nanoparticles made of silver oxy salt (Ag_7NO_{11}) and silver arsenate (Ag_3AsO_4) at the semiconductor/electrolyte interface if the GaAs wafer is illuminated by the X-ray and reaction time is long enough.

KEYWORDS Time-resolved X-ray diffraction, in situ probing, galvanic reaction, silver nanoplates

Semiconductor/electrolyte interfaces are important in a broad range of applications including photovoltaics (e.g., photoelectrochemical cells),[1−3] photocatalysis,[4,5] and chemical/biological sensing.[6,7] If a semiconductor is reactive toward an electrolyte that is in contact with the semiconductor, reaction(s) at the semiconductor/electrolyte interface might result in the formation of nanoparticles on the semiconductor to modify properties of the interface, thus affecting its performance. For example, illuminating TiO_2 nanoparticles immersed in a solution of noble metal ions with ultraviolet (UV) light can induce photoreduction of metal ions on the TiO_2 surfaces, resulting in the deposition of metal nanoparticles on the TiO_2 nanoparticles.[8] Placing an n-type semiconductor wafer (e.g., Si, GaAs, InP, Ge) in contact with an aqueous solution of noble metal ions (e.g., $AgNO_3$, $AuCl_4^-$, $PtCl_6^{2-}$) usually initiates a spontaneous galvanic reaction between the wafer and the metal ions, leading to the deposition of metal nanoparticles on the surface of the wafer.[9−12] Modification of the semiconductor surfaces with metal nanoparticles can significantly influence charge transfer processes and chemical reactions at the semiconductor/electrolyte interfaces when the composite semiconductors are used as functional components in the aforementioned applications.[4,13−16] In general, effect of the metal nanoparticles strongly relies on their size, morphology, composition, and crystalline structure, which are determined by the reaction conditions and growth time.[17] As a result, developing time-resolved techniques that are capable of in situ probing the evolution of nanoparticles formed from reactions at semiconductor/electrolyte interfaces is very important for understanding the dependence of nanoparticles on the reaction conditions as well as for controlling the parameters and properties of the resulting nanoparticles. In the past decade, many *in situ* experiments have been attempted by monitoring the variation of tailorable properties (e.g., optical absorption and scattering, electrical conductivity) of the nanoparticles. However, intrinsic parameters (e.g., crystalline structure, chemical environment, size, and shape) of the nanoparticles that determine their tailorable properties are difficult to probe in the real time because characterizing these parameters usually requires high vacuum techniques (such as electron microscopy and X-ray photoelectron spectroscopy) that are not compatible with liquid electrolytes. Most recently, thin cells have been specially designed for studying liquid samples in transmission electron microscope (TEM).[18,19] Preliminary results show that this in situ TEM technique can monitor variations of nucleation population and particle size during the growth of nanoparticles. The obtained images, however, cannot reveal the detailed structural and morphological information of the nanoparticles.

* To whom correspondence should be addressed. E-mail: ygsun@anl.gov.
Received for review: 07/14/2010
Published on Web: 08/03/2010

DOI: 10.1021/nl102458k | *Nano Lett.* **2010,** *10,* 3747–3753

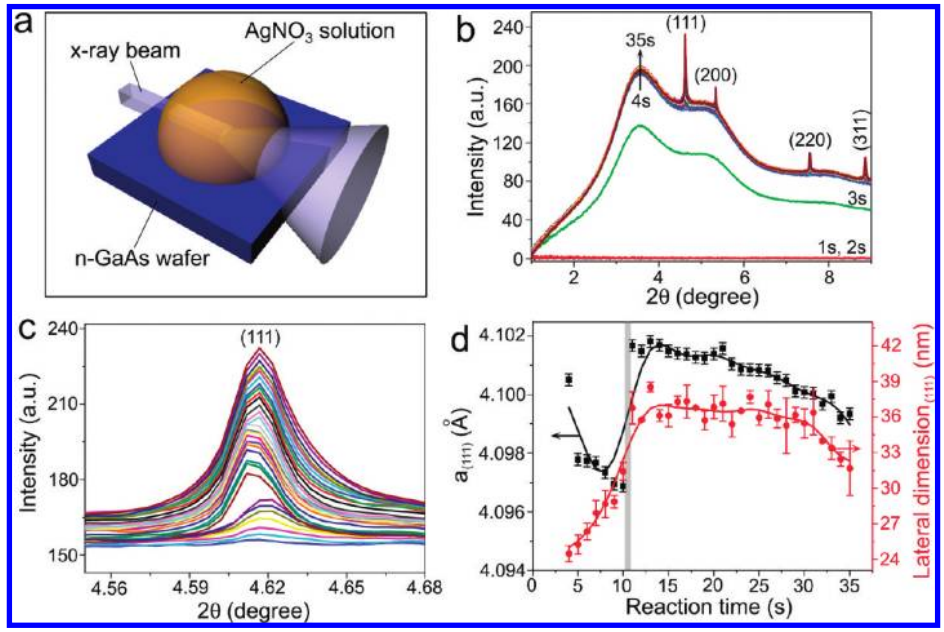

FIGURE 1. (a) Schematic illustration of the experimental setup for in situ monitoring the evolution of nanoparticle growth at the interface formed between an n-type GaAs wafer and an aqueous solution of $AgNO_3$ with concentration of 1.5 M at room temperature. (b,c) Time-dependent synchrotron X-ray diffraction patterns of the Ag nanoparticles grown on the n-type GaAs wafer, clearly showing the structural and morphological evolution involved in the interfacial reaction within 35 s. (d) Variation of the lattice constant that was calculated from position of the (111) peak and the lateral dimension of the Ag nanoparticles along their (111) crystalline directions that was calculated from peak width of the (111) peak as a function of reaction time. The X-ray beam constantly illuminated the GaAs-wafer/$AgNO_3$-solution interface and the integration time for acquiring each diffraction pattern was 1 s. Wavelength of the X-ray beam was 0.1907 Å.

Furthermore, the reaction kinetics within the small volume of the cell chambers deviate substainitially from those developed for large-scale synthesis in ambient environments. As a result, probes that can deeply penetrate liquid electrolytes in ambient environments are critical for in situ monitoring of nanoparticle growth at semiconductor/electrolyte interfaces. High-energy synchrotron X-rays represent such an ideal class of probes because they can efficiently penetrate liquid electrolytes. The corresponding time-resolved techniques (such as small-angle X-ray scattering,[20,21] X-ray absorption spectroscopy,[22,23] wide-angle X-ray scattering[24−27]) show the potential for real-time monitoring nanoparticle growth in liquid media. However, these studies have yet to be used to resolve kinetics at the vicinity of semiconductor/electrolyte interfaces, due in large part to the low volume concentration of nanoparticles at the interfaces. In this letter, we report that the use of focused, high-flux ($\sim 10^{11}$ photons/s), high-energy (65.02 keV), wide-angle X-ray diffraction provides structural information for real-time monitoring of nanophase evolution with a time resolution of 1 s at the interface formed between GaAs wafers and an aqueous solution of $AgNO_3$ at room temperature.

Our previous studies on the galvanic reactions between single-crystalline GaAs wafers and aqueous solutions of $AgNO_3$ have illustrated many important aspects in growth of anisotropic nanoparticles at the GaAs/$AgNO_3$-solution interface.[28−30] For example, placing a drop of $AgNO_3$ solution with concentration higher than 1 M on an highly doped n-type GaAs wafer leads to the deposition of pure Ag nanoplates with flat surfaces on the GaAs substrate within several minutes (Supporting Information Figure S1a).[29] The nanoplates protrude out of the surface of the GaAs substrate and exhibit uniform thickness that can be tuned in the range of 20−160 nm by controlling the concentration of $AgNO_3$. Structural characterization based on ex situ X-ray diffraction (XRD, Supporting Information Figure S1b), selected area electron diffraction (SAED, Supporting Information Figure S1c), and high-resolution transmission electron microscopy (HRTEM) images (Supporting Information Figure S1d) reveals that each nanoplate is a face-centered cubic (fcc) single crystal with the basal surfaces bounded by {111} facets and with multiple twin planes parallel to the basal surfaces.[31] However, the structural and dimensional variations of the Ag nanocrystals that are critical for understanding growth mechanism of the anisotropic nanoplates have not been observed yet during the galvanic reaction. In this work, we try to tackle this challenge by exploiting the ability of high-energy synchrotron X-rays to penetrate the $AgNO_3$ solution and study nanocrystals deposited at the GaAs/solution interface. Wide-angle X-ray diffraction provides precise structural information (derived from diffraction peak pattern and position) and approximate dimensional information (derived from diffraction peak width and area). Figure 1a illustrates the experimental setup. A 1 × 1 cm^2 n-type GaAs wafer (doped with Si at a concentration of $\sim 1.7 \times 10^{18}$ cm^{-3}, surface orientation along (100) crystalline direction) that has been precleaned by soaking in a 2% HF aqueous solution followed by rinsing with plenty of deionized (DI) water is

DOI: 10.1021/nl102458k | Nano Lett. 2010, 10, 3747–3753

horizontally placed on a sample stage. A 65 keV synchrotron X-ray beam focused down to a size of 60 μm (h) × 40 μm (v) having a flux of $\sim 10^{11}$ photons/s is aligned to be parallel to the surface of the GaAs wafer. The beam vertically intersects the surface of the wafer such that half of the beam hits the wafer and half travels above the wafer. Once the beam shutter is opened, a drop of aqueous $AgNO_3$ solution (with concentration of 1.5 M) is delivered to the wafer surface via a remotely controlled syringe pump (Figure 1a). X-ray diffraction patterns are then recorded with intervals of 1 s and the time scale is normalized against the time when the beam shutter is opened. Figure 1b plots a series of XRD patterns obtained from 0 to 35 s. Essentially no signal is observed at 2 s and shorter times, indicating that the orientation of the single crystalline GaAs wafer is well aligned to eliminate the appearance of diffraction spots and the surface of the GaAs wafer is clean. Strong signals with broad peaks start to appear at 3 s when the droplet of $AgNO_3$ solution is delivered to the surface of the wafer. Contact between the GaAs wafer and the $AgNO_3$ solution immediately initiates galvanic reaction and the corresponding growth of Ag nanoparticles, as witness by the appearance of peaks of fcc Ag at 4 s. Intensities of the diffraction peaks associated with this phase increase with reaction time up to 35 s, indicating that the X-ray beam does not significantly influence the interfacial galvanic reaction at this early stage. As a result, these initial Ag nanoparticles may exhibit platelike morphologies similar to the nanoplates (Supporting Information Figure S1) previously found to form in the absence of X-rays. Detailed analysis on the diffraction patterns is consistent with this argument. As shown in Figure 1c (blowup of the (111) peaks), intensity of the peaks monotonically increases with the reaction time up to 11 s when a big jump occurs and the corresponding peak position exhibits a sudden shift to a lower 2θ value. Lattice constants (a) and lateral dimensions of the Ag nanocrystals along the (111) direction are calculated according to the peak positions and peak widths shown in Figure 1c and the corresponding data are plotted in Figure 1d. The lattice constant slightly decreases with reaction time at the very beginning of the reaction (≤10 s) and jumps to a much larger value (i.e., 4.1017 Å) at 11 s followed by a slight decrease at longer reaction times (>11 s). Meanwhile, the lateral dimension of the Ag nanocrystals along their (111) direction monotonically increases until 11 s and then remains essentially constant from 11 to 30 s, indicating that the Ag nanocrystals grow into plates with a constant thickness of ~35 nm after 11 s. The drastic change of lattice constant and lateral dimension from 10 to 11 s suggests that transition from the nucleation stage for the Ag nanoplates to the growth stage occurs within a very short period <1 s (i.e., from 10 to 11 s) (highlighted by the gray strip in Figure 1d). At the nucleation stage (i.e., 3−10 s), Ag atoms generated from the reaction between GaAs and $AgNO_3$ condense on the surface of the GaAs wafer to form small Ag clusters (i.e., nuclei). Once the size of the nuclei increases to a critical value, they may undergo a spontaneous structural transformation to form nanoparticles containing multiple twin planes parallel each other, which serve as seeds for the growth of Ag nanoplates. Formation of the multiple twin planes in the seeds accounts for the sudden increase in lattice constant of the fcc Ag. As a result, forming a Ag nanoplate at the GaAs/electrolyte interface includes three sequential steps: (i) nucleation process with gradual increase of the size of a nucleus; (ii) quick structural transformation of the nucleus to form a seed with multiple, parallel twin planes within 1 s; (iii) growth process with gradual increase of the size of the seed to form a nanoplate. The results, for the first time, directly show the good separation between nucleation and growth stages involved in the structural evolution of the Ag nanoplates. In addition, the results also reveal that a quick transition step exists between the nucleation and growth stages. The transition is critical for structural transformation of the nuclei to form seeds needed for anisotropic growth of the nuclei into nanoplates.

Although the effect of X-ray irradiation on the GaAs substrate and the growth of Ag nanoplates is negligible at short reaction times (i.e., < 35 s), charge separation in the GaAs lattices is expected to be induced at longer times. This can correspondingly influence reactions at the GaAs/electrolyte interface, resulting in the formation of new nanoparticles. For example, silver oxy salt, $Ag(Ag_3O_4)_2NO_3$ (or Ag_7NO_{11}) starts to appear at 35 s and silver arsenate (Ag_3AsO_4) starts to form at 60 s. Figures 2a,b clearly shows the development of new diffraction peaks associated with these two phases with increase of the reaction time. All diffraction peaks recorded in the course of 0−200 s can be well indexed to fcc Ag, fcc Ag_7NO_{11},[32] and simple cubic (sc) Ag_3AsO_4 with the cubic groups of $Fm\bar{3}m$, $Fm\bar{3}m$, and $P\bar{4}3n$, respectively (Supporting Information Figure S2). Previous studies show that X-ray irradiation can create charge separation in an n-type GaAs substrate although the mechanism is different from absorption of visible light.[33] In general, X-ray photons with high energies excite deep core levels of elements in the GaAs lattice followed by relaxation through Auger process or secondary photon emission, which creates a cascade of secondary electrons, holes, and photons.[34,35] These secondary electrons and holes eventually thermalize to the band edges of the GaAs wafer (i.e., electrons in the conduction bands and holes in the valence bands). The holes and electrons accumulated at the band edges can either recombine to emit photons (or phonons) or diffuse at the GaAs/electrolyte interface to induce chemical reactions before they recombine. At the early stage of the reaction, the n-type GaAs wafer has high concentration of surface electrons that can quickly recombine with the holes generated from absorption of the X-ray. As a result, influence of the probe X-ray on the growth of Ag nanoplates is not significant when the reaction time is less than 35 s. When the reaction time is long enough (>35 s), surface electrons of the GaAs

DOI: 10.1021/nl102458k | Nano Lett. 2010, 10, 3747–3753

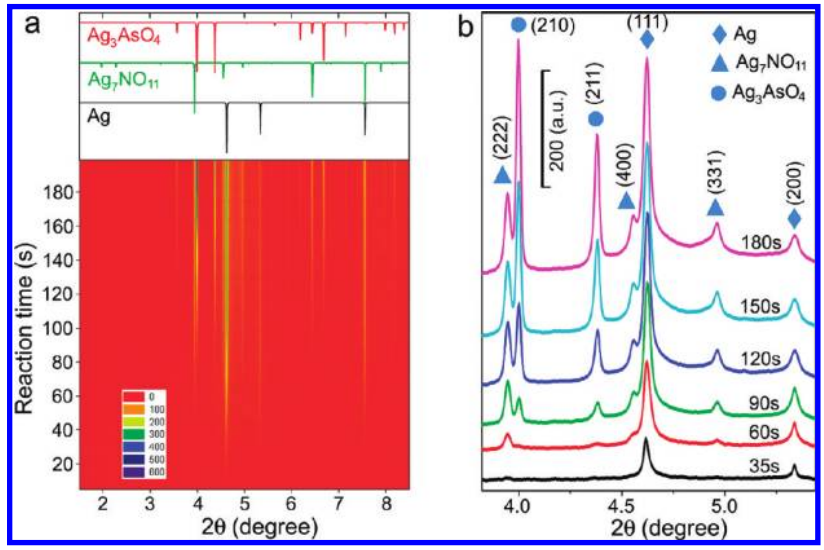

FIGURE 2. (a) X-ray diffraction patterns of the products grown at the GaAs-wafer/$AgNO_3$-solution interface shown in Figure 1a continuously recorded with a time interval of 1 s. For visual clarity, signals of all the diffraction patterns obtained at time ≥4 s are subtracted by that of the pattern obtained at 4 s to eliminate the strong background originated from the $AgNO_3$ solution. Standard powder X-ray diffraction patterns of fcc Ag, fcc Ag_7NO_{11}, and sc Ag_3AsO_4 are also plotted as references. (b) Diffraction patterns at a number of specific times focusing in the range of $3.82° < 2\theta < 5.44°$, clearly showing the appearance of new peaks with increase of reaction time. The major peaks are well indexed and labeled. The curves are intentionally offset to enhance visual clarity. Other conditions are the same as those of Figure 1.

wafer are consumed during the growth of Ag nanoplates. The X-ray induced holes then have a longer lifetime to diffuse at the GaAs/electrolyte interface to drive possible reactions: (i) oxidation of the Ag nanoplates, resulting in the formation of geometric defects in the nanoplates (Supporting Information Figure S3); (ii) oxidation of $AgNO_3$ to form Ag_7NO_{11} nanoparticles; and (iii) oxidation of GaAs and oxides (i.e., Ga_2O_3 and As_2O_3)[36] to release AsO_4^{3-} ions into the $AgNO_3$ solution, leading to a precipitation reaction between AsO_4^{3-} and Ag^+ ions to form Ag_3AsO_4 nanoparticles. Meanwhile, the leftover electrons reduce Ag^+ ions to induce the formation of new Ag nanoparticles on the surface of the GaAs wafer, which is consistent with the increased intensity of the diffraction peaks for Ag (Figure 2b).

Detailed analysis over the major diffraction peaks of Ag, Ag_7NO_{11}, and Ag_3AsO_4 (i.e., (111) for Ag, (222) for Ag_7NO_{11}, and (210) for Ag_3AsO_4) are summarized in Figure 3. As shown in Figure 3a, these phases are all in the form of nanoparticles with lateral dimensions less than 50 nm. As previously discussed in Figure 1, products formed at the early stage (i.e., <35 s) of the reaction are dominated by Ag nanoplates with thickness of ~35 nm on the surface of the GaAs wafer. The average lateral dimension of the Ag nanoparticles along their (111) directions decreases to ~25 nm at longer time (>35 s) while the corresponding area under the Ag(111) peak that is proportional to the overall mass of the Ag nanoparticles continuously increases with reaction time (Figure 3b). This opposite trend for lateral dimension and peak area indicates that more and more Ag nanoparticles with smaller sizes of ~25 nm are formed as the reaction time is elongated. The increase of peak area follows a sigmoidal (Boltzmann) relationship as a function of reaction time (solid squares in Figure 3b), indicating that the growth of Ag nanoparticles occurs on the surface of the GaAs wafer.[29] The time-dependent variation of peak area for Ag_7NO_{11} follows a similar sigmoidal function, indicating that the growth of Ag_7NO_{11} nanoparticles also takes place on

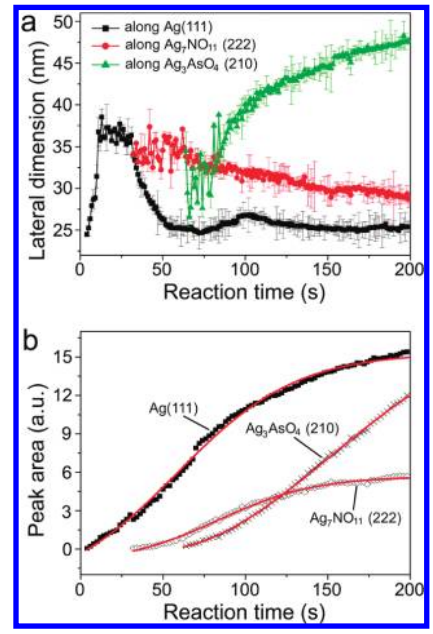

FIGURE 3. Dependence of (a) lateral dimensions of the nanoparticles along the specific crystalline directions and (b) integrated peak area on the reaction time. All the results were calculated according to the diffraction patterns shown in Figure 2. The time (t) dependent peak area (A) shown in (b) can be fitted with (red curves): $A = 15.366 + (-3.443 - 15.366)/(1 + e^{(t\ -\ 58.870)/36.292})$ for the (111) peak of Ag; $A = 5.695 + (-1.179 - 5.695)/(1 + e^{(t-83.528)/29.636})$ for the (222) peak of Ag_7NO_{11}; and $A = -3.494 + 0.0385t + 2.06 \times 10^{-4}t^2$ for the (210) peak of Ag_3AsO_4.

DOI: 10.1021/nl102458k | *Nano Lett.* **2010,** *10,* 3747–3753

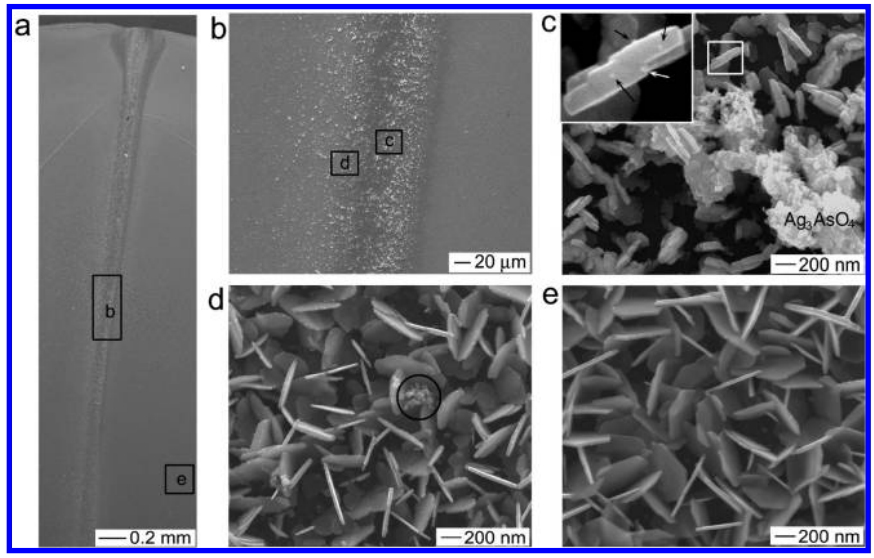

FIGURE 4. SEM images of the nanoparticles grown at the GaAs-wafer/$AgNO_3$-solution interface shown in Figure 1a after the reaction and measurement lasted 200 s. Frames (b-e) correspond to the magnified images of the areas highlighted in the black boxes labeled with the same letters. The inset of (c) is a blowup image of the nanoplate highlighted by the white box in (c).

surfaces of solid substrates. As shown in Figure 4c,d, the silver oxy salt nanoparticles (i.e., the small bright spots) grow on the surfaces of the Ag nanoplates. In contrast, the increase of peak area for Ag_3AsO_4 behaves in a different way, that is, second order polynomial regression model, indicating that the Ag_3AsO_4 nanoparticles may be formed in the solution phase adjacent to the GaAs/electrolyte interface through the precipitation reaction between Ag^+ ions and AsO_4^{3-} ions. Overall, the formation of nanoparticles at long reaction times (i.e., >35 s) is ascribed to the electrons and holes generated from illumination of the X-ray beam. As a result, the amount of the nanoparticles decreases when the illumination time of the X-ray is decreased (Supporting Information Figure S4 versus Figure 2b). Oxidation reactions for the formation of Ag_7NO_{11} and Ag_3AsO_4 can occur only when species (e.g., Ag^+ ions) that can be reduced by the X-ray-induced electrons are available at the GaAs/electrolyte interface. For example, continuously irradiating a GaAs substrate covered with Ag nanoplates (Supporting Information Figure S1) cannot induce the formation of new material phases when the sample is immersed in pure water (Supporting Information Figure S5). In addition, the oxidative species that are responsible for the formation of Ag_7NO_{11} and Ag_3AsO_4 are not produced from X-ray radiolysis of water. When a continuous X-ray beam is located completely above the GaAs substrate and still passes through the $AgNO_3$ solution, no diffraction peaks of Ag_7NO_{11} and Ag_3AsO_4 can be detected during the reaction although the diffraction peaks of Ag can be observed (Supporting Information Figure S6). SEM characterization of this sample shows that nanoparticles deposited on the surface of the GaAs wafer are mainly dominated by Ag nanoplates.

Figure 4 presents a series of scanning electron microscopy (SEM) images of the sample obtained through the reaction shown in Figure 1a for 200 s at room temperature under continuous illumination of an X-ray beam. The low-magnification images (Figure 4a,b) clearly show that the illuminated surface area (i.e., the strip in the middle of the images) of the GaAs substrate through which the X-ray passes exhibits a contrast against the other areas, confirming that the X-ray irradiation does affect the growth of nanoparticles at the GaAs-wafer/$AgNO_3$-solution interface. The nanostructures observed in the central region of the strip can be classified into four categories: nanoplates on the GaAs surface, small nanoparticles on the GaAs surface, small nanoparticles on the surfaces of the nanoplates, and aggregates of nanoparticles over the nanoplates. The nanoplates are made of Ag, similar to the Ag nanoplates grown on the area without illumination of the X-ray (Figure 4e) except that they have smaller sizes. The difficulty to enlarge the nanoplates into larger ones in the illuminated area is ascribed to that the holes induced by the X-ray can prevent the hole inject process that is the major driving force for the growth of nanoplates.[31] In addition, the holes are also able to diffuse through the GaAs-wafer/Ag-nanoplate interfaces into the Ag nanoplates to oxidize them, leading to the formation of geometric defects in the nanoplates (Supporting Information Figure S3a). The small nanoparticles on the surface of the GaAs substrate are also made of Ag and formed through reduction of Ag^+ ions by the electrons generated from illumination of the X-ray. The small nanoparticles on the Ag nanoplates are believed to be composed of Ag_7NO_{11} although no direct evidence is available at this moment. Previous studies show that Ag_7NO_{11} crystals can be epitaxially deposited on solid substrates through photooxidation (or electrochemical oxidation) of $AgNO_3$.[37−39] Given the fact that the (400) and (622) lattices of Ag_7NO_{11} are very close to the (111) and (220) lattices of Ag, Ag_7NO_{11} nanoparticles may grow epitaxially on the surface of the Ag nanoplates under the present experimental conditions. As

DOI: 10.1021/nl102458k | *Nano Lett.* **2010,** *10,* 3747–3753

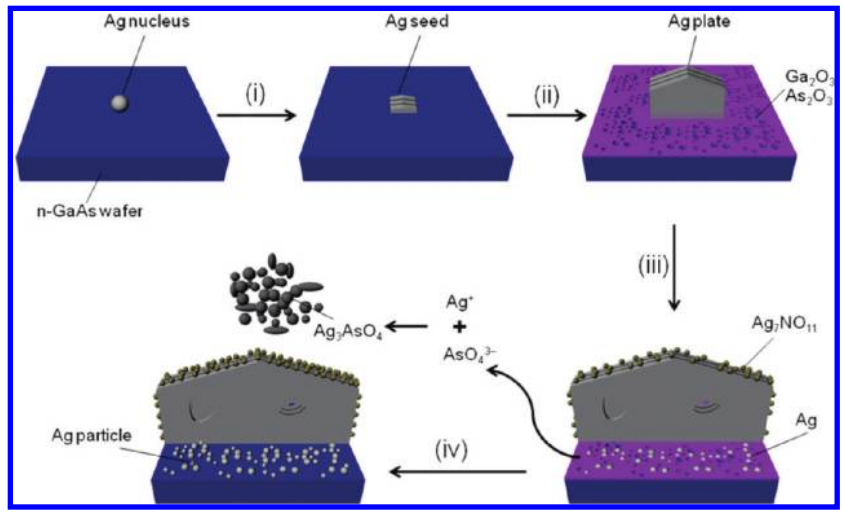

FIGURE 5. Mechanism involved in the growth of nanoparticles at the GaAs-wafer/$AgNO_3$-solution interface under constant illumination of an X-ray beam. The porosity of the purple layer indicates that the oxide film formed during the growth of Ag nanoplates is amorphous.

highlighted in the inset of Figure 4c, the number of the Ag_7NO_{11} nanoparticles on the side surfaces (highlighted by arrows) is much higher than that on the basal surfaces, which is ascribed to the higher surface energy associated with the side surfaces. The large nanoparticle aggregates are found to be composed of Ag_3AsO_4 (Supporting Information Figure S3b,c). It is worth noting that the width of the strip in Figure 4a is slightly larger than that of the X-ray beam, indicating the charges generated from illumination of the X-ray beam can diffuse to the adjacent regions in the GaAs wafer before they recombine. As a result, nanoparticles made of Ag_7NO_{11} and Ag_3AsO_4 can also be found in the area that is not illuminated with the X-ray but is close to the illuminated area. Figure 4d presents a typical SEM image of nanostructures formed in such an area, clearly showing the existence of small Ag_7NO_{11} nanoparticles on the side surfaces of Ag nanoplates and aggregates of Ag_3AsO_4 nanoparticles (highlighted by the circle).

According to these observations (Figures 1−4), nanophase evolution at the semiconductor/electrolyte interface formed between an n-type GaAs wafer and an aqueous $AgNO_3$ solution can be summarized in Figure 5 when the interface is partially illuminated with a focused, high-energy synchrotron X-ray beam. In the illuminated region, Ag atoms are produced through reduction of Ag^+ ions with surface electrons in the GaAs wafer once the $AgNO_3$ solution (not shown here) contacts the wafer and condense on the wafer surface to form small Ag clusters (or nuclei); this process is called the nucleation process. The size of the nuclei continuously increases with reaction time while their crystalline structures may fluctuate between fcc phases with different defects. Once the size of each nucleus reaches a critical value, it experiences a quick structural reconstruction to form a stable particle containing multiple (111) twin planes parallel to each other, which serves as a seed for the growth of a nanoplate (step i). The seeds can be quickly enlarged into nanoplates with the confinement of the multiple twin planes in the following growth process, which is dominated by a hole injection process responsible for reduction of Ag^+ ions (step ii).[31] The hole injection process can simultaneously produce oxides (i.e., As_2O_3 and Ga_2O_3, highlighted by the porous purple layer) on the surface of the GaAs wafer.[36] The well separation between nucleation and growth processes is important for the growth of anisotropic nanoparticles with well-defined shapes.[17] The transition from the nucleation to the growth process occurs very quickly (i.e., < 1 s). When the reaction time is short (i.e., < 35 s), the X-ray irradiation has negligible influence on the growth of Ag nanoplates because of the existence of high concentration of surface electrons in the GaAs wafer. As a result, the mechanism depicted in Figure 5 is suitable for interpreting the growth of Ag nanoplates on n-type GaAs wafer regardless of reaction conditions. Once the surface electrons are consumed during the growth of Ag nanoplates, electrons and holes generated from illumination of X-ray can accumulate at the band edges of the GaAs wafer to induce additional reactions before they recombine. The electrons accumulated in the conduction band can reduce Ag^+ ions around the GaAs-wafer/$AgNO_3$-solution interface to form more Ag nanoparticles (steps iii and iv). On the other hand, holes accumulated in the valence band can diffuse through the GaAs-wafer/Ag-nanoplate interfaces into the Ag nanoplates to drive two possible reactions: oxidation of the Ag nanoplates to form geometrical defects (e.g., pores, rough surfaces, etc.) and oxidation of $AgNO_3$ to deposit Ag_7NO_{11} nanoparticles on the surfaces of the Ag nanoplates (step iii). The holes can also diffuse in the GaAs substrate to the surface area without Ag nanoparticles to oxidize the GaAs lattices as well as the oxide layer formed during the growth of Ag nanoplates, leading to the release of AsO_4^{3-} ions into the $AgNO_3$ solution. Precipitation reaction between AsO_4^{3-} and Ag^+ ions results in the formation of Ag_3AsO_4 nanoparticles in the solution adjacent to the

DOI: 10.1021/nl102458k | *Nano Lett.* **2010,** *10,* 3747–3753

GaAs/electrolyte interface (step iv). Because of the absence of surfactant molecules in the $AgNO_3$ solution, the Ag_3AsO_4 nanoparticles usually aggregate into larger chunks.

In summary, a time-resolved diffraction technique based on focused, high-energy synchrotron X-ray beams has been successfully developed to in situ study the evolution of complex nanophases at the semiconductor/electrolyte interfaces formed between GaAs wafers and aqueous $AgNO_3$ solutions. The results for the first time clearly distinguish between the nucleation and growth stages involved in the structural evolution of the anisotropic Ag nanoplates on the GaAs substrates. Nanoparticles made of Ag_7NO_{11} and Ag_3AsO_4 are also formed at the semiconductor/electrolyte interfaces due to the oxidation reactions driven by the holes generated from the X-ray irradiation. In contrast, direct reactions between the GaAs wafers and $AgNO_3$ solutions in the absence of X-rays result in the formation of nanoparticles only with pure phase of fcc Ag. The difference indicates that high-energy X-rays can be used to pattern semiconducting wafers with nanoparticles which are difficult to produce through conventional chemical reactions. The capability of this technique to probe nanophase evolution in real-time and at semiconductor/electrolyte interfaces, as demonstrated in this work, suggests that it has a great promise for studying nanoparticle growth at solid/liquid interfaces and in homogeneous solutions.

Acknowledgment. Use of the Center for Nanoscale Materials, Advanced Photon Source, and the Electron Microscopy Center for Materials Research at Argonne was supported by the U.S. Department of Energy, Office of Science, Office of Basic Energy Sciences, under Contract No. DE-AC02-06CH11357.

Supporting Information Available. Figures S1−S6. This material is available free of charge via the Internet at http://pubs.acs.org.

REFERENCES AND NOTES

(1) Boettcher, S. W.; Spurgeon, J. M.; Putnam, M. C.; Warren, E. L.; Turner-Evans, D. B.; Kelzenberg, M. D.; Maiolo, J. R.; Atwater, H. A.; Lewis, N. S. *Science* **2010**, *327*, 185.
(2) Gratzel, M. *Nature* **2001**, *414*, 338.
(3) Hochbaum, A. I.; Yang, P. *Chem. Rev.* **2010**, *110*, 527.
(4) Linsebigler, A. L.; Lu, G.; Yates, J. T., Jr. *Chem. Rev.* **1995**, *95*, 735.
(5) Qu, Y.; Liao, L.; Cheng, R.; Wang, Y.; Lin, Y.-C.; Huang, Y.; Duan, X. *Nano Lett.* **2010**, *10*, 1941.
(6) Gao, X. P. A.; Zheng, G.; Lieber, C. M. *Nano Lett.* **2010**, *10*, 547.
(7) Cohen-Kami, T.; Timko, B. P.; Weiss, L. E.; Lieber, C. M. *Proc. Natl. Acad. Sci. U.S.A.* **2009**, *106*, 7309.
(8) Li, D.; McCann, J. T.; Gratt, M.; Xia, Y. *Chem. Phys. Lett.* **2004**, *394*, 387.
(9) Chai, J.; Wang, D.; Fan, X.; Buriak, J. M. *Nat. Nanotechnol.* **2007**, *2*, 500.
(10) Aizawa, M.; Cooper, A. M.; Malac, M.; Buriak, J. M. *Nano Lett.* **2005**, *5*, 815.
(11) Magagnin, L.; Maboudian, R.; Carraro, C. *J. Phys. Chem. B* **2002**, *106*, 401.
(12) Sun, Y.; Wiederrecht, G. P. *Small* **2007**, *3*, 1964.
(13) Lombardi, I.; Marchionna, S.; Zangari, G.; Pizzini, S. *Langmuir* **2007**, *23*, 12413.
(14) Nishijima, Y.; Ueno, K.; Yokota, Y.; Murakoshi, K.; Misawa, H. *J. Phys. Chem. Lett.* **2010**, *1*, 2031.
(15) Tian, Y.; Tatsuma, T. *J. Am. Chem. Soc.* **2005**, *127*, 7632.
(16) Standridge, S. D.; C., S. G.; Hupp, J. T. *J. Am. Chem. Soc.* **2009**, *131*, 8407.
(17) Xia, Y.; Xiong, Y.; Lim, B.; Skrabalak, S. E. *Angew. Chem., Int. Ed.* **2009**, *48*, 60.
(18) Zheng, H.; Smith, R. K.; Jun, Y.-W.; Kisielowski, C.; Dahmen, U.; Alivisatos, A. P. *Science* **2009**, *324*, 1309.
(19) Williamson, M. J.; Tromp, R. M.; Vereecken, P. M.; Hull, R.; Ross, F. M. *Nat. Mater.* **2003**, *2*, 532.
(20) Abecassis, B.; Testard, F.; Spalla, O.; Barboux, P. *Nano Lett.* **2007**, *7*, 1723.
(21) Polte, J.; Erler, R.; Thunemann, A. F.; Sokolov, S.; Ahner, T. T.; Rademann, K.; Emmerling, F.; Kraehnert, R. *ACS Nano* **2010**, *4*, 1076.
(22) Chen, C.-H.; Sarma, L. S.; Chen, J.-M.; Shih, S.-C.; Wang, G.-R.; Liu, D.-G.; Tang, M.-T.; Lee, J.-F.; Hwang, B.-J. *ACS Nano* **2007**, *1*, 114.
(23) Harada, M.; Inada, Y. *Langmuir* **2009**, *25*, 6049.
(24) Cheong, S.; Watt, J.; Ingham, B.; Toney, M. F.; Tilley, R. D. *J. Am. Chem. Soc.* **2009**, *131*, 14590.
(25) Middelkoop, V.; Boldrin, P.; Peel, M.; Buslaps, T.; Barnes, P.; Darr, J. A.; Jacques, D. M. *Chem. Mater.* **2009**, *21*, 2430.
(26) Bremholm, M.; Felicissimo, M.; Iversen, B. B. *Angew. Chem., Int. Ed.* **2009**, *48*, 4788.
(27) Bremholm, M.; Becker-Christensen, J.; Iversen, B. B. *Adv. Mater.* **2009**, *21*, 3572.
(28) Sun, Y. *Chem. Mater.* **2007**, *19*, 5845.
(29) Sun, Y.; Yan, H.; Wiederrecht, G. P. *J. Phys. Chem. C* **2008**, *112*, 8928.
(30) Sun, Y.; Pelton, M. *J. Phys. Chem. C* **2009**, *113*, 6061.
(31) Sun, Y. *J. Phys. Chem. C* **2010**, *114*, 857.
(32) Naray-Szabo, I.; Argay, G.; Szabo, P. *Acta Crystallogr.* **1965**, *19*, 180.
(33) Sun, Y.; Yan, H.; Wu, X. *Appl. Phys. Lett.* **2008**, *92*, 183109.
(34) Soh, Y.-A.; Aeppli, G.; Zimmermann, F. M.; Isaacs, E. D.; Frenkel, A. I. *J. Appl. Phys.* **2001**, *90*, 6172.
(35) Ma, Q.; Noldovan, N.; Mancini, D. C.; Rosenberg, R. A. *Appl. Phys. Lett.* **2000**, *77*, 1319.
(36) Sun, Y.; Lei, C.; Gosztola, D.; Haasch, R. *Langmuir* **2008**, *24*, 11928.
(37) Takahashi, R.; Katayama, M.; Dahl, O.; Grepstad, J. K.; Matsumoto, Y.; Tybell, T. *Appl. Phys. Lett.* **2009**, *94*, 232901.
(38) Michailova, E.; Milchev, A. A. *J. Appl. Electrochem.* **1988**, *18*, 614.
(39) Breyfogle, B. E.; Phillips, R. J.; Switzer, J. A. *Chem. Mater.* **1992**, *4*, 1356.

DOI: 10.1021/nl102458k | *Nano Lett.* **2010,** *10,* 3747--3753